Features of the formation and propagation of plasma diffuse jets

NIKITA VINOGRADOV, VICTOR TARASENKO, EVGENII BAKSHT, DMITRY SOROKIN
Laboratory of Optical Radiations
Institute of High Current Electronics SB RAS
Tomsk, 2/3 Akademichesky Avenue
RUSSIAN FEDERATION

Abstract: - Plasma diffuse jets (PDJ) with a length of over 100 cm were generated using a capacitive discharge in a quartz tube with ring electrodes. It was determined that the electrode installation location of ring electrodes does not affect the characteristics of PDJ in air and nitrogen. It was established that PDJ emissions primarily consist of the (1+) and (2+) nitrogen bands. When spectra were recorded in the interelectrode region, the (1−) nitrogen bands also appeared in the spectrum. At pressures below 0.1 Torr, spectral lines from the dissociation products of water vapor (CO, OH, and H) emerged, affecting the discharge plasma glow color. Spectra of PDJ were obtained at lower frequencies than those previously studied. At a frequency of 1 Hz, no discharge formation was observed. However, as the frequency increased to 1 kHz, PDJ began to form. It was found that the PDJ color was redder at negative voltage pulse polarity than at positive one, as confirmed by emission spectra from the diffuse jet body. It was shown that within the range of 3 to 21 cm from the outer edge of the ring electrode, the velocity of the first ionization wave (IW) propagating to the left of the electrodes was lower than that of the IW propagating to the right. This phenomenon is explained by a decrease in plasma potential with increasing distance from the high-voltage electrode due to the finite conductivity of the discharge plasma, as the registration region on the left was farther from the high voltage electrode than the corresponding region on the right.

Key-Words: - Red sprites; Experimental modeling; Streamer discharge in air

Received: May 2, 2025. Revised: July 16, 2025. Accepted: August 17, 2025. Published: November 1, 2025.

1 Introduction

Atmospheric discharges observed at altitudes from 20 to 100 km above sea level [1, 2] are called "transient luminous events" (TLE). TLEs include red sprites [1-4], blue jets [5-8], elves [9-12], halos [13-16] and other types of high-altitude discharges. The most common type of TLE are red sprites. They usually appear over mesoscale convective systems and are light flashes of red color that occur because of electrical discharges in the mesosphere above thunderclouds, see, for example, [1-4]. Red sprites are initiated at the altitude of about 70 km and propagate both toward the Earth's surface (up to the altitude of about 50 km) and in the opposite direction (up to the altitude of about 100 km). The first documented observation of red sprites dates to the publication of black-and-white photographs in 1990 [9]. Observations from space [10-12] and from an airplane [17-20] soon followed. The shape of red sprites is very diverse and depends on many conditions. Key results concerning them were published in the following articles and monographs [3-4, 11, 13]. Fig. 1 demonstrates a photograph of column red sprites taken from the surface of the Earth, analogues of which is experimentally modeled in this work.

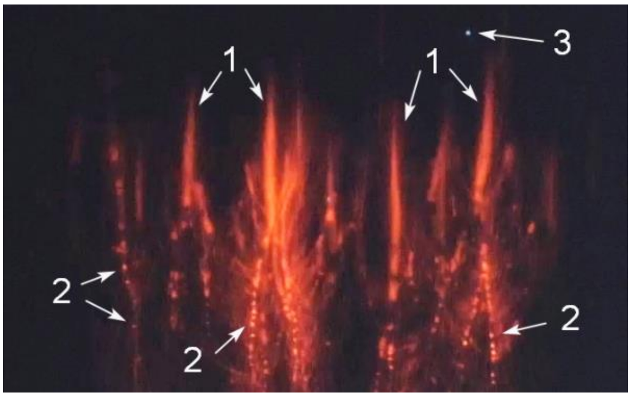

Fig. 1: Photo of red sprites captured in Cabo Rojo, Puerto Rico (September 28, 2020, at 04:59:14 UTC). 1 – “main channels” of column sprites; 2 – “beads”; 3 – bright star

The photograph shows that the column sprites at the top consist of parallel cylinders (1) and then turn into separate beads (2). The sprites are tens of kilometers in dimensions and are photographed from the Earth at great distances (usually more than 100 km). This is necessary so that clouds located below do not interfere the field of view. It has now been established that the propagation of column sprites is associated with a streamer breakdown mechanism, see, for example, [3, 5, 7, 17].

2 Problem Formulation

In addition to studying red sprites in natural conditions, attempts are being made to model them experimentally [21-24] and using computer simulation [25-28]. For example, one of the studies involves experimental modeling of red sprites using the Large Plasma Facility [21] in air, where a discharge is ignited between tip and plane electrodes. In this experiment, the discharge plasma contacts the metal of the electrodes. In another work [22], red sprites are also simulated, where the tip-plane electrodes are in contact with the plasma. One more experiment can be mentioned [24], in which red sprites are also simulated in a long tube, but the authors did not prevent plasma-electrodes metal contact. Contact between the plasma and electrodes is present in all listed papers [21-24]. The problem is that in real conditions of red sprite formation, there are no electrodes, and, accordingly, there is no contact between the electrode metal and the plasma.

A feature of our work is the use of a capacitive discharge to simulate red sprites. The use of the capacitive discharge allows us to avoid plasma contact with the electrode metal, which brings our experimental model closer to the real conditions of red sprite formation.

This comparison reveals a notable similarity across several key parameters. Both phenomena exhibit a characteristic red color, primarily due to emissions in the same spectral bands, namely the first positive (FPS (1+)) and second positive (SPS (2+)) systems of nitrogen, which is a hallmark of sprite discharges [4, 12, 20–22]. Their propagation velocities are also comparable, with sprites ranging from 0.4 to 1.7 times 10 to the seventh power meters per second [4, 12, 20–22] and PDJs measured between 1.2 and 1.7 times 10 to the seventh power meters per second [29]. The plasma conditions show convergence as well: the electron temperature is approximately 1–2 eV for sprites [4, 12, 20–22] and around 2.5 eV for PDJs [29], while the reduced electric field strength for sprites spans a wide range from tens to thousands of Townsends [4, 12, 20–22] and is specifically about 350 Td for PDJs [29]. The most significant difference lies in the operational pressure, with sprites occurring at much lower pressures between 3 and 2.4 times 10 to the minus fourth power Torr [4, 12, 20–22], compared to PDJs which were studied at higher pressures ranging from 3 to 0.4 Torr [29].

The aim of the work is to obtain new data on the properties of miniature analogues of column red sprites. Using a pulse-periodic capacitive discharge formed in a quartz tube at low-pressure air, the spectral characteristics of radiation in the main areas of the discharge were studied at voltage pulse repetition rates from 10 Hz to 21 kHz. Data on the speed of the streamers that form plasma diffuse jets were obtained.

3 Problem Solution

To study plasma diffuse jets initiated by the capacitive discharge at low pressures of air and other gases, setup was created. The photograph of the setup is shown in Fig. 2.

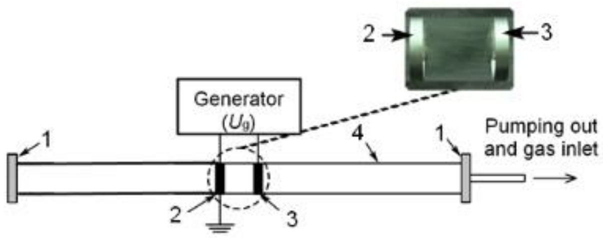

Fig. 2: Experimental setup for studying PDJs induced by the capacitive discharge: 1 – caprolon flanges; 2 – grounded electrode; 3 – high-voltage electrode; 4 – quartz tube. Electrodes 2 and 3 were mounted on the outer surface of the quartz tube and were ring-shaped.

The discharge was ignited in a tube made of GE-214 quartz, which has high transmittance in the ultraviolet (UV), visible and near infrared (IR) regions of the spectrum. The length of the tube and its internal diameter were 230 cm and 5 cm, respectively. Flanges made of caprolon were mounted on the ends of the tube.

The relative humidity of the air in the room during the experiments was ≈ 25%. A high-voltage generator was used that formed voltage pulses of positive or negative polarity with the adjustable pulse repetition rate f. In most experiments, the voltage pulse repetition rate was f = 21 kHz. The amplitude of the voltage pulse formed by the generator was ≈ 7 kV with a FWHM of ≈ 1.5 μs.

The voltage across the discharge gap was measured by an AKTAKOM ACA-6039 divider with resistances of 900 kOhm and 900 MOhm. The discharge current was determined by a shunt with a resistance of 3 Ohm. The signals from the divider and shunt were recorded with an MDO 3104 oscilloscope (1 GHz, sampling frequency of 5 samples/ns). Optical radiation of the discharge plasma in the tube was captured by a Canon 2000D digital camera, HR2000+ES (range 200–1150 nm; optical resolution ≈ 0.9 nm) and HR4000 (range 300–400 nm; optical resolution ≈ 0.2 nm) spectrometers with known spectral sensitivities, and a silicon photomultiplier (SiPM) as part of the MicroFC-SMA-10035 module. The pulses and radiation spectra were recorded through a 0.5 or 1 cm wide slit using an optical fiber. The optical fiber was located at different distances from the edge of the ring electrode along the longitudinal axis of the tube.

3.1 Effect of pulse repetition rate

In our previous works, investigations of the PDJ properties were carried out mainly at the generator pulse repetition rate of 21 kHz [29-32]. In this section, the possibility of obtaining a red PDJ with a decrease in f is shown. In the general case, it is possible to implement a breakdown of long tubes in the ionization wave (streamer) formation mode with single voltage pulses [33]. This is achieved by increasing the voltage pulse amplitude and (or) decreasing the gas pressure, as well as by reducing the distance between the electrodes and (or) increasing the exposure. In this section, discharge ignition was studied at various frequencies on setup #1. At the air pressure p = 1 Torr and a frequency of 1 Hz, the discharge was not formed, although the voltage across the electrodes increased to 10 kV. This followed from the integral photographs of the tube and the waveforms of the current and voltage. The breakdown between the ring electrodes, registered visually and with the camera, occurred at a pulse frequency of about 10 Hz, but the radiation intensity was very weak and photographs in the dark required an exposure of at least 30 s. In addition, the shape of the discharge differed from that observed at higher pulse repetition rates. At p = 1 Torr and the low f, the discharge diameter (transverse dimension) approximately corresponded to the internal diameter of the quartz tube. Under similar conditions, at the f = 21 kHz, see, for example, [29], the diameter of the PDJ decreased with the distance from the ring electrodes. Therefore, measurements were carried out at f of about 1 kHz and more.

Normalaized to single pulse spectral distributions of radiation energy density are shown in Fig. 3a, b.

(*a*)

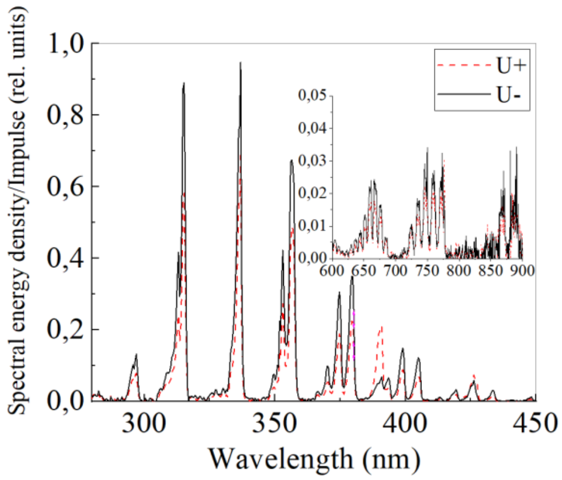

(*b*)

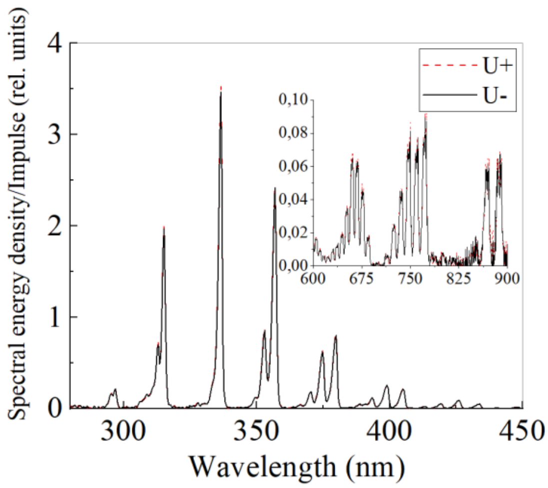

Fig. 3: Radiation energy density distributions, normalized to single pulse, for two polarities of voltage pulses at frequencies of 3 kHz (a) and 21 kHz (b). Radiation was recorded from a point shifted 11 cm from the right edge of the grounded ring electrode.

The emission spectra from a point located at the distance of 11 cm from the right ring electrode were successfully recorded at frequencies from 1 to 21 kHz. At f from 1 to 10 kHz, the influence of the voltage pulse polarity on the emission spectra compound and the color of a PDJ was studied. At a lower frequency, the lower intensity of the discharge plasma emission made impossible the signal to be recorded. Also, the dependence of the ratio of the integrals by the energy density per pulse in the blue and red color ranges on f was determined, see Table 1.

Table 1. Dependence of the ratio of the total energy of the emission bands in the blue W (380–500 nm) region to the red W (630–780 nm) region of colors at different polarities of voltage pulses.

	Pulse frequency, kHz			
	1	3	10	21
blue / red for U+	4.17	5.17	5.23	3.85
blue / red for U-	1.49	4.13	4.94	3.84

The ratios of radiation energies in the blue and red ranges from show a large relative share of radiation energy in the 630–780 nm range over the radiation energy in the 380–500 nm range with negative polarity of voltage pulses. A similar feature is manifested at frequencies less than 10 kHz, respectively, a predominance of the red color was observed with negative polarity of the voltage pulse. A comparison of the energy density per pulse in the blue and red ranges was carried out for all the frequencies studied. At f from 10 to 21 kHz, a similar phenomenon ceases to appear both in photographs and in the radiation spectra. The ratio of the integrals by the energy density per pulse does not change with a change in the voltage pulse polarity, Fig. 3(b).

Waveforms of discharge current and voltage at the pulse repetition frequency of 10 Hz and 21 kHz are shown in Fig. 4.

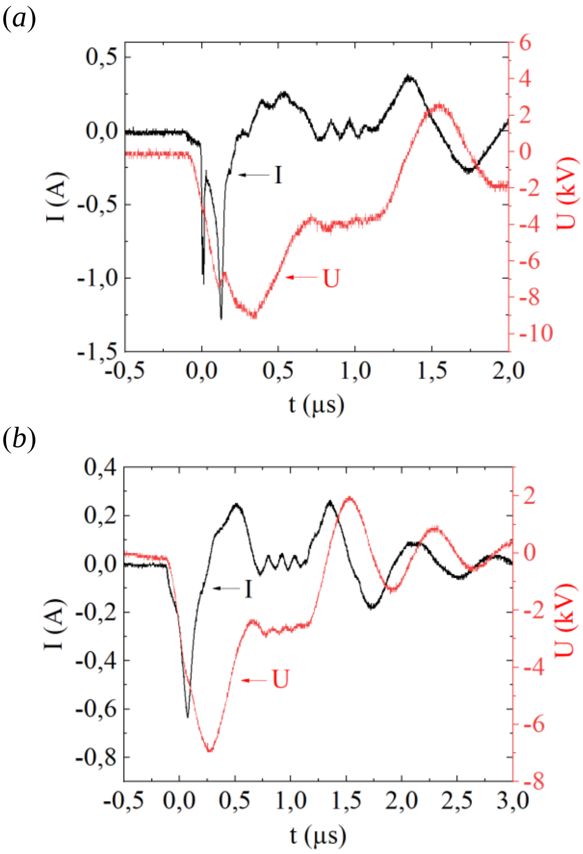

Fig. 4: Waveforms of the discharge current and voltage at negative polaritiy of voltage pulses at f of 10 Hz (a) and 21 kHz (b)

The comparison was carried out at the maximum investigated frequency (21 kHz) and the minimum one (10 Hz). As shown above, at 10 kHz, the radiation energy in the 630–780 nm region was predominant over the radiation energy in the 380–500 nm region with negative polarity of the voltage pulses. It turned out that the current and voltage waveforms for these frequencies differ significantly. Thus, at a frequency of 10 Hz, two peaks were recorded during the first current pulse, while at a frequency of 21 kHz, only one peak was recorded. The first current peak at f = 10 Hz can be associated with gas breakdown in the interelectrode region. The second peak of the current pulse at both frequencies is associated with the propagation of a PDJ from the plasma formation region.

3.2 Measuring the ionization wave velocity

In the experiments, the front velocity of a PDJ consisting of two streamers [31] was measured using a silicon photomultiplier (SiPM). Note that when studying discharges in long tubes, a streamer is usually called an ionization wave (IW) [31, 33]. Both terms reflect the same phenomenon. Both a streamer and an ionization wave can be attributed to the moving region of ionization created by a high electric field, since the physical processes during their formation are similar. In this paper, we will use the term streamer, since it is used to describe column red sprites [15].

To record the radiation, a silicon photomultiplier (SiPM) was used as part of the MicroFC-SMA-10035 module, into which the discharge plasma radiation entered through the optical fiber. The receiving end of the optical fiber was equipped with a collecting lens and was located at 10 cm from the surface of the quartz tube. The measurements were carried out in a discharge region limited in width at distances x = 3, 11, 21 and 31 cm from the outer edge of the ring electrode to the nearest edge of the region under study both on the right and on the left side of these electrodes on setup #1. The discharge region under study was limited on both sides by opaque screens made of black paper placed on the tube and was 1 cm in width. Waveforms of the voltage on the electrodes, the current through the shunt and the SiPM signal are shown in Fig. 5.

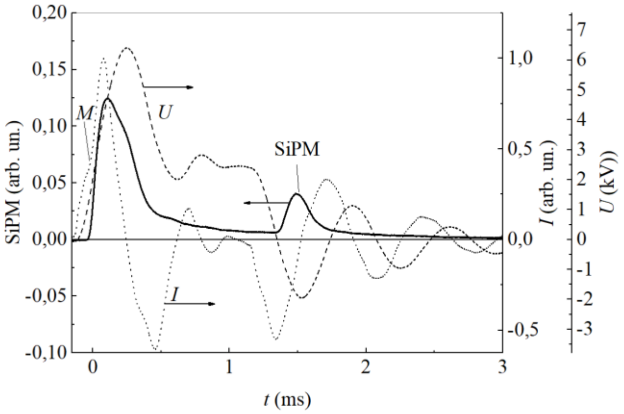

Fig. 5: Waveforms of the SiPM signal, voltage U on the electrodes and current I through the shunt. x = 11 cm from the right (potential) electrode. f = 21 kHz. Averaging over 64 pulses.

The plasma radiation intensity waveform has two characteristic peaks corresponding to the largest voltage drops across the electrodes and the discharge current flow. These peaks are recorded for all four studied distances from the outer edge of the electrodes both to the right and to the left of the electrodes. Their time delay relative to the discharge current increases with increasing distance from the electrodes, which indicates the spread of the glow from the electrodes both to the right and to the left of them. We associate this with the spread of the glow to the sides from the electrodes, associated with the propagation of the streamers and charging of the walls of the quartz tube.

The moment of appearance of characteristic pulses (peaks) of glow is determined by the presence of the required potential gradient at the plasma boundary between the electrodes and the region external to the electrodes. For the first glow peak, this moment is close to the beginning of the conduction current in the region between the electrodes (point M in Fig. 5, at which the rate of current growth noticeably increases), and for the second peak — to the moment when the plasma between the electrodes reaches its maximum concentration (near the maximum conduction current in the discharge)

The values of the propagation velocities of the first and second streamers in different regions of the PDJ are shown in Fig, 6. When calculating the velocity, the time intervals between the fronts of the corresponding pulses were measured at the half of the amplitude (level 0.5).

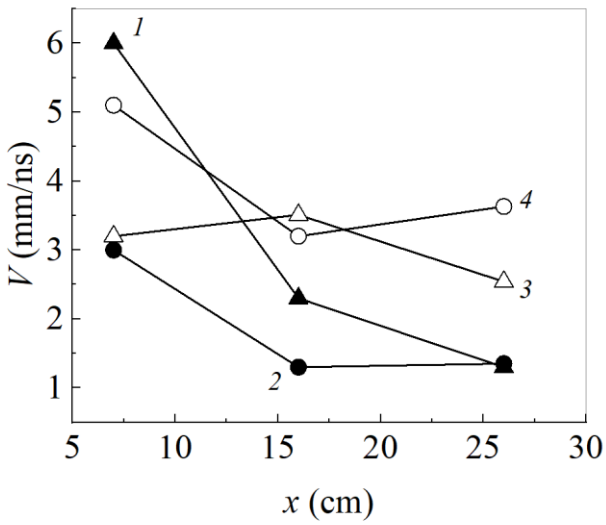

Fig. 6: Propagation velocities of the first and second streamers in different regions of the PDJ. The abscissa axis shows the distances corresponding to the middles of these regions (intervals 3–11, 11–21 and 21–31 cm both on the right and left sides of the outer edge of the electrodes). 1, 2 – velocity of the first IW; 3, 4 – velocity of the second IW; 1, 3 – velocity of IW to the right of the electrodes; 2, 4 – to the left of the electrodes. f = 21 kHz. Averaging over 64 pulses.

It is evident that in the first and second regions the velocity of the first streamer (the first glow peak in Fig. 5), propagating to the left from the electrodes, is lower than that of the IW propagating to the right. This is explained by the decrease in the plasma potential with distance from the potential electrode due to the finite conductivity of the discharge plasma and by the fact that for the outer left region of the discharge with respect to the electrodes the points at which the plasma radiation was recorded are further removed from the potential electrode than for a similar region on the right. The velocity values in the third region (interval 21–31 cm from the outer edge of the ring electrode) on the right and in the second (interval 11–21 cm from the outer edge of the ring electrode) and third region on the left are approximately the same and amount to ~1.3 mm/ns. One of two options can be assumed: 1) the potential gradient at the streamer front and the electron concentration before it is respectively close in value in these sections, or 2) the electron concentration ne0 in front of the streamer front decreases, but as a result, the potential gradient at its front increases (the value of lf decreases). Apparently, the first option is realized for the third region of the PDJ on the right and the second region of the PDJ on the left, and the second option is realized for the second and third regions of the PDJ on the left.

The dependences of the second streamer velocities on the distance to the right and left of the electrodes are more complex than for the first streamer. Their dynamics are determined by the electron concentration in the recombining plasma ahead of the streamer front in different regions of the PDJ and the potential gradient at the front, which depends on several factors, including the aforementioned electron concentration. The higher value of the streamer velocity for the outer left discharge region in relation to the electrodes in the first region of the PDJ (interval 3–11 cm from the outer edge of the ring electrode) compared to the right is explained by the lower plasma concentration at the time of the second streamer start, which leads to a decrease in lf. In the remaining regions of the PDJ, the value of the velocities is also determined by the ratio of such parameters as the potential difference Δφ, the reduced length of the electric field in the streamer front lf, the electron concentration ahead of the front ne0, and the distance xf. In addition, the value of the velocity is affected by the residual charge of the tube walls, which can be different in different regions of the PDJ.

4 Conclusion

The results obtained in this study provide additional information on the characteristics of a PDJ formed between ring electrodes at different air pressures and voltage pulse repetition rates. The results are consistent with previous studies [29, 30-32] and expand the understanding of the discharge behavior at lower frequencies and pressures.

Designate the area between the ring electrodes as the first area, and the near-electrode area as the second area. It is shown that in the first and second regions the velocity of the first IW propagating to the left of the electrodes is less than that of the IW propagating to the right. This is explained by a decrease in the plasma potential with distance from the potential electrode due to the finite conductivity of the discharge plasma and by the fact that for the outer left region of the discharge with respect to the electrodes the points at which the plasma radiation was recorded are further removed from the potential electrode than for a similar region on the right. The velocity values in the third region on the right and in the second and third regions on the left are approximately the same and amount to ~1.3 mm/ns. Such behavior may be since the potential gradient at the IW front and the electron concentration ahead of its front are, respectively, close in value in these regions, or the electron concentration ne0 in front of the IW front decreases, but as a result the potential gradient at the IW front increases.

The dependences of the second ionization wave (IW) velocities on the distance to the left and right of the electrodes are more complex compared to the first IW. Their dynamics are determined by the electron concentration in the recombining plasma ahead of the IW front in different regions of the PDJ, as well as the potential gradient at the front, which in turn depends on many factors, including the specified electron concentration. For example, in the first region of the PDJ, the second IW velocity for the outer left region of the discharge exceeds the same velocity on the right. This is explained by the lower plasma concentration at the start of the second IW, which leads to a decrease in the front length.

In other regions of the PDJ, the velocity of the second IW is determined by a set of parameters, such as the potential difference Δφ, the front length lf, the electron concentration before the front ne0 and the distance xf. In addition, the residual charge on the tube walls, which can vary in different sections of the PDJ, also affects the wave velocity. The relationship between all these parameters is complex, so for a more accurate analysis of the dependencies presented in Fig. 6, it is necessary to conduct additional studies, including computer modeling of the discharge processes.

The discharge behavior at low repetition rates (≤ 10 kHz) showed that the formation of PDJs is sensitive to the polarity and frequency of the applied voltage. At 1 Hz, no discharge ignition was observed, which is due to insufficient energy input to maintain the discharge. At 1 kHz, PDJs were formed, but with differences in color between the positive and negative voltage polarities. In particular, the red color was predominant for the negative polarity, which is confirmed by the ratios of the spectral energy density between the blue and red regions. This effect was reduced at higher frequencies (≥ 10 kHz), where the dependence of the spectral characteristics on polarity was not evident.

During this study, it was shown that with the help of the capacitive discharge it is possible to form PDJs, that having properties corresponding to the plasma of red sprites, that the formation of PDJs occurs at frequencies from 1 to 21 kHz.

It has been found that the spectral characteristics of the discharge in characteristic areas and the integral photographs of the discharge radiation are similar for the circuit with ring and flat electrodes.

References:

[1] Sentman D.D., Wescott, E.M., Red sprites and blue jets: Thunderstorm- excited optical emissions in the stratosphere, mesosphere, and ionosphere, *Physics of Plasmas*, Vol. 2, No. 6, 1995, pp. 2514–2522.

[2] Rodger C.J., Red sprites, upward lightning, and VLF perturbations, *Reviews of Geophysics*, Vol. 37, No. 3, 1999, pp. 317–336.

[3] Pasko V.P., Red sprite discharges in the atmosphere at high altitude: the molecular physics and the similarity with laboratory discharges, *Plasma Sources Science and Technology*, Vol. 16, No. 1, 2007, pp. S13–S13.

[4] Williams E., Valente M., Gerken E., Golka R., Sprites, Elves and Intense Lightning Discharges, *Springer*, 2006, pp. 237–251.

[5] McHarg M.G., Stenbaek-Nielsen H.C., Kammae T., Observed emission rates in sprite streamer heads, *Geophysical Research Letters*, Vol. 34, No. 6, 2007, pp. L06804.

[6] Kanmae T., Stenbaek-Nielsen H.C., McHarg M.G., Haaland R.K., Diameter-speed relation of sprite streamers, *Journal of Physics D: Applied Physics*, Vol. 45, No. 27, 2012, pp. 275203.

[7] Pasko V.P., Yair Y., Kuo C.L., *Space Science Reviews*, Vol. 168, No. 1, 2012, pp. 475–516.

[8] Singh M., Sharma P.K., Pathak P.P., Radiation Phenomenon Due to Streamers of Sprites, *Journal of Electromagnetic Analysis and Applications*, Vol. 14, No. 3, 2022, pp. 31–37.

[9] Franz R.C., Nemzek R.J., Winckler J.R. Television Image of a Large Upward Electrical Discharge Above a Thunderstorm System, *Science*, Vol. 249, No. 4964, 1990, pp. 48–51.

[10] Garipov G.K., Khrenov B.A., Klimov P.A., Global transients in ultraviolet and red-infrared ranges from data of Universitetsky-Tatiana-2 satellite, *Journal of Geophysical Research: Atmospheres*, Vol. 118, No. 2, 2013, pp. 370–379.

[11] Jehl A., Farges T., Blanc E., Color pictures of sprites from non-dedicated observation on board the International Space Station, *Journal of Geophysical Research: Space Physics*, Vol. 118, 2013, pp. 454–461.

[12] Neubert T., Ostgaard N., Reglero V., The ASIM Mission on the International Space Station, *Space Science Reviews*, Vol. 215, No. 2, 2019, pp. 1–17.

[13] Neubert T., Rycroft M., Farges T., Recent Results from Studies of Electric Discharges in the Mesosphere, *Surveys in Geophysics*, Vol. 29, No. 2, 2008, pp. 71–137.

[14] Stenbaek-Nielsen H.C., Haaland R., McHarg M.G., Sprite initiation altitude measured by triangulation, *Journal of Geophysical Research: Space Physics*, Vol. 115, No. A8, 2010, pp. A00E16.

[15] Qin J., Celestin S., Pasko V.P., Mechanism of column and carrot sprites derived from optical and radio observations, *Geophysical Research Letters*, Vol. 40, No. 17, 2013, pp. 4777–4782.

[16] Malagon-Romero A., Teunissen J., Stenbaek-Nielsen H.C., On the emergence mechanism of carrot sprites, *Geophysical Research Letters*, Vol. 47, No. 9, 2020, pp. e2019GL085776.

[17] Pasko V.P., Qin J., Celestin S., Toward Better Understanding of Sprite Streamers: Initiation, Morphology, and Polarity Asymmetry, *Surveys in Geophysics*, Vol. 34, No. 6, 2013, pp. 797–830.

[18] Vaughan O.H., Jr., Blakeslee R., Broeck W.L., Vonnegut B., Brook M., McKune J., Jr., A cloud-to-space lightning as recorded by the space shuttle payload bay camera, *Monthly Weather Review*, Vol. 120, No. 6, 1992, pp. 1459–1461.

[19] Sentman D.D., Wescott E.M., Observations of atmospheric optical flashes recorded from an aircraft, *Geophysical Research Letters*, Vol. 20, No. 24, 1993, pp. 2857–2860.

[20] Williams E.R. Sprites Elves, Glow Discharge Tubes, *Physics Today*, Vol. 54, No. 11, 2001, pp. 41–47.

[21] Evtushenko A.A., Gushchina M.E., Korobkova S.V., Strikovskiya A.V., Mareeva E.A., Simulation of High-Altitude Discharges in a Large Plasma Facility, *Geomagnetism and Aeronomy*, Vol. 60, No. 3, 2020, pp. 345–354.

[22] Briels T.M.P., van Veldhuizen E.M., Ebert U., Positive streamers in air and nitrogen of varying density: experiments on similarity laws, *Journal of Physics D: Applied Physics*, Vol. 41, No. 23, 2008, pp. 234008.

[23] Arcanjo M., Montanyà J., Urbani M., Lorenzo V., Optical Signatures Associated With Streamers and Leaders of Laboratory Discharges, *Geophysical Research Letters*, Vol. 48, No. 22, 2021, pp. e2021GL095601.

[24] Anikin N.B., Zavialova N.A., Starikovskaia S.M., Starikovskii A.Y., Nanosecond-Discharge Development in Long Tubes, *IEEE Transactions on Plasma Science*, Vol. 36, No. 4, 2008, pp. 1142–1143.

[25] Singh M., Sharma P.K., Pathak P.P., Radiation Phenomenon Due to Streamers of Sprites, *Journal of Electromagnetic Analysis and Applications*, Vol. 14, No. 3, 2022, pp. 31–37.

[26] Jiang F., Huang C., Wang Y., Emission spectrum of sprites caused by the quasi‐electrostatic field above thunderstorm clouds, *Meteorology and Atmospheric Physics*, Vol. 131, No. 5, 2019, pp. 1253–1261.

[27] Kuo C.-L., Williams E., Adachi T., Ihaddadene, K., Celestin, S., Experimental Validation of N2 Emission Ratios in Altitude Profiles of Observed Sprites, *Frontiers in Earth Science*, Vol. 9, 2021, pp. 687989.

[28] Malagón-Romero A., Teunissen J., Stenbaek-Nielsen H.C., McHarg M.G., Ebert U., Luque A., On the emergence mechanism of carrot sprites, *Geophysical Research Letters*, Vol. 46, No. 17-18, 2019, pp. 10207–10215.

[29] Tarasenko V.F., Vinogradov N.P., Baksht E.Kh., Sorokin D.A., Experimental Simulation of Red Sprites in a Laboratory, *Journal of Atmospheric Science Research*, Vol. 5, No. 3, 2022, pp. 26-36.

[30] Tarasenko V.F., Sosnin E.A., Skakun V.S., Panarin V.A., Trigub M.V., Evtushenko, G.S., *Physics of Plasmas*, Vol. 24, No. 4, 2017, pp. 043514.

[31] Sosnin E.A., Panarin V.A., Skakun V.S., Tarasenko V.F., Kuznetsov V.S., *Applied Physics*, No. 1, 2017, pp. 21.

[32] Chanrion O., Neubert T., Production of runaway electrons by negative streamer discharges, *Journal of Geophysical Research: Space Physics*, Vol. 115, No. A3, 2010, pp. A00E32.

[33] Ionikh Y.Z., Electric breakdown in long discharge tubes at low pressure, *Plasma Physics Reports*, Vol. 46, No. 10, 2020, pp. 1015–1044.

Contribution of Individual Authors to the Creation of a Scientific Article (Ghostwriting Policy)

The authors equally contributed in the present research, at all stages from the formulation of the problem to the final findings and solution.

Sources of Funding for Research Presented in a Scientific Article or Scientific Article Itself

This study was carried out with the financial support of the Russian Science Foundation through grant No. 24-29-00166

Conflict of Interest

The authors have no conflicts of interest to declare that are relevant to the content of this article.